香港教育大學
The Education University of Hong Kong

A Project entitled

Synthetic Non-heme Iron catalyst for C-H bond halogenation

submitted by

WANG WENDUO

submitted to The Education University of Hong Kong

for the degree of *Bachelor of Education (Honors) (Science)*

in April 2022

Declaration

I, *WANG WENDUO* declare that this research report represents my own work under the supervision of *Professor (Practice) CHOW Cheuk Fai Stephen* and that it has not been submitted previously for examination to any tertiary institution.

Signature: _____

Date: 2022/04/08

Keywords: tetracoordinate, iron(III) complex, synthetic model, C-H halogenation

Abstract: In the natural condition, hydroxylation is preferred over halogenation due to the involvement of molecular oxygen. Halogenation in the inner bio-environment requires a complex co-effect of enzyme chains or groups, which is hard to simulate in artificial reactions. Thus, developing an effective and selective model for halogenation is important for synthetic chemistry study. This project proposed synthetic iron(III) complexes for C-H halogenation. Ligands based on 6-(Aminomethyl)-2,2'-bipyridine were synthesized and identified, while corresponding iron(III) complexes were examined.

Acknowledgment: Over the course of my research and writing this paper, I would like to express my thanks to all those who have helped me. Prof. Chow provided me the insights into the research topic and experimental design. Andy and Huey in the EdUHK research lab taught me plentiful practical skills in experiment operation and supported me to carry out the project. On go, Ramen and other lab technicians ensured me fluent usage of various instruments in the laboratory, so that I could generate and interpret valid results and information. It’s been a long wish of mine to study something interesting and it’s a fortune that it was fulfilled in the last year of my bachelor program. Thanks again to all those who supported me in this project.

Table of contents

1. Introduction

1.1 Background

Oxygen, no doubt the foundation of the current earth environment, has various unique features due to its high oxidation potential and electron configuration. Living creatures had developed numerous physiological mechanisms to utilize oxygen since the origin of life billions of years ago. The development of modern science revealed that oxygen utilization is largely related to cofactors containing transition metals such as iron, copper, and occasionally magnesium. The mechanism of natural enzymes utilizing oxygen was further analyzed and developed for C-H halogenation.

1.2 Problem statement

Hydroxylated and halogenated hydrocarbons are of great importance in organic synthesis, pharmaceuticals, chemical biology, and materials science. However, the functionalization of aliphatic C–H bonds via direct C–H bond activation has been a long-standing challenge, as C-H σ-bonds have relatively high stability. In the early stages, toxic heavy metals or strong oxidants were used yet the severe pollution to the environment and the compromise of selectivity indicated a better synthetic pathway was needed.

Hydroxylation of unactive C-H bond was generally discovered earlier than halogenating reaction as it's a thermodynamically preferred pathway according to the radical rebound theory (Srnec & Solomon, 2017). Two major enzyme families observed and analyzed in the past few decades would be focused on in this study. **1.** Cytochrome P450 (CYP) family functions as the monooxygenase of organic substrates. The heme-iron(III) cofactor of CYP is thought to be the active site, in which the iron is tetradentate to a heme group ligand. **2.** The alpha-ketoglutarate-dependent (αKG-dependent) hydroxylases are comparable to CYP enzymes, but the metal center is iron(II) and is normally coordinated by two histidine residues

and one aspartic acid/glutamic acid residue. The rest three coordination sites are occupied by αKG and oxo-group for catalytic reactions (Hausinger, 2004).

The utilization of natural enzyme models was not enough satisfying. Bio-systems have a high requirement of the reaction condition and the mechanism is harder to be determined with the involvement of large complex molecules such as proteins. Therefore, synthetic biomimetic models were proposed. Furthermore, by adjusting the models with the structure or reaction condition, selective halogenation of the aliphatic C-H bond was also achieved. Recent models largely lowered the halogenating reaction's required condition, which gave researchers more chances to reveal the principle and mechanism of radical rebound reactions.

1.3 Research questions and hypothesis

This study aimed at developing synthetic models with a planar-tetradentate structure to selectively catalyze the C-H bond halogenation. Planar-tetradentate ligands were proposed, synthesized, and identified. Then iron complexes were synthesized and examined with their catalytical performances. Such models proposed in this study were expected to obtain higher efficiency and selectivity of halogenation and higher tolerance to the thermal condition.

2. Literature review

2.1 Theoretical foundation of C-H bond activation: radical rebound mechanism

C-H bond activation was considered a relatively difficult process as it has a high bond dissociation energy. To activate the C-H bond artificially, normally requires harsh conditions such as high temperature or high pressure. Studies had revealed that various enzymes were adopted in the biological systems to achieve such difficult reactions by forming a high-valent metal-oxide complex as the intermediate. Among these enzymes, cytochrome P450 was focused on by chemists for processing the oxo-iron-porphyrin complex in it (Morimoto, 2019).

The role of cytochrome P450 in the hydroxylation of aliphatic C-H bonds was widely agreed to be forming 2 intermediates that involve the valance change of the center metal ion. Hydroxyl radical is formed and rebounded to the carbon radical in such a process(Puri et al., 2016). Thus, this is also referred to as the 'radical rebound' mechanism.

The catalytical cycle consisted of 2 stages: at first, the cytochrome P450 is activated by oxidants such as H_2O_2 and forms an Oxoiron(IV) complex, normally referred to as the *compound I*; then the Oxoiron(IV) center catalyzes the Hydrogen Atom Abstraction *(HAA)* from the substrate and forms [Fe^{IV}–OH·R], referred to as the *compound II*; in the end, the hydroxide radical will rebound to the incipient substrate radical and forms the hydroxylated product(Huang & Groves, 2017).

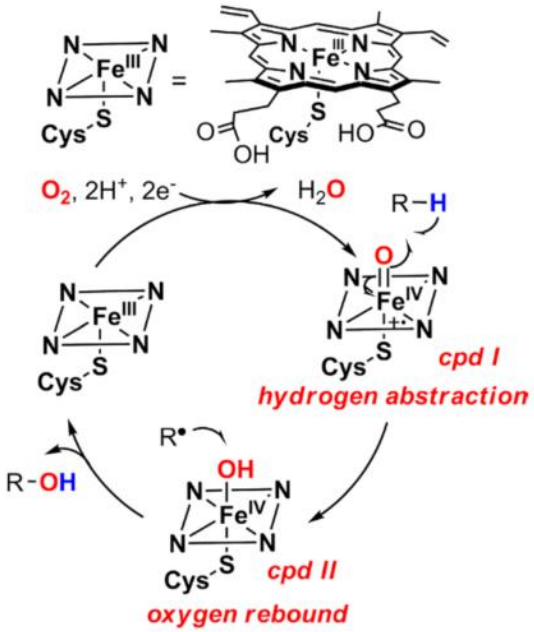

Fig. 1 Mechanism of aliphatic C–H hydroxylation catalyzed by cytochrome P450

Another example is the typical αKG dependent non-heme iron(II) dioxygenases, TauD. The mechanism of TauD is analogous to that of P450s. In the first stage, the high-valent oxoiron(IV) intermediate is formed by the oxidant (O_2), similar to P450 cpd I. Then it abstracts the hydrogen from the substrate and forms the hydroxo-iron intermediate, similar to P450 cpd II. In the end, the substrate radical rebounds to the hydroxyl group and affords the hydroxylated product.

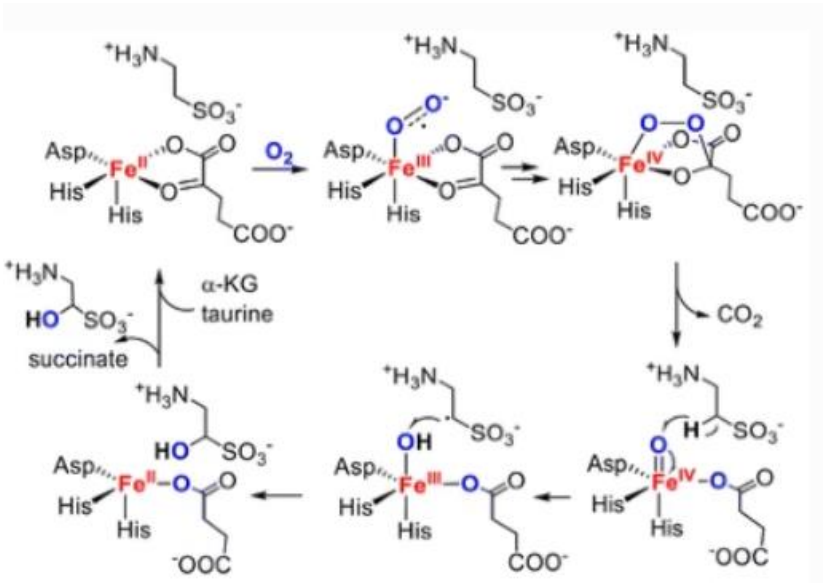

Fig. 2 Mechanism of taurine hydroxylation catalyzed by TauD

2.2 Heme-metal models and their ramifications for C-H activation

After the observation of the *compound, I* formed from cytochrome P450, the reaction and application of it were extensively studied. Synthetic and biomimetic models were proposed to achieve highly efficient and selective alkane hydroxylation. Yet most of the studies in this stage focused on the hydroxylation of the C-H bond, not halogenation. To implement the radical rebound approach for other C-H bond functionalization, a standing challenge was that the oxygenation products formed via hydroxyl group rebound must be suppressed.

2.2.1 Heme manganese complexes

The halogenation effect was first observed in the study of manganese porphyrin complexes, Mn^{III}(TPP)(Cl/Br). It was suggested that the oxo-manganese(V) species were the key reactive intermediates (Groves, 1980). Later on, Hill and co-workers proved that manganese-porphyrin complexes with various axial ligands including chloride, bromide, iodide, and azide could activate and functionalize the C-H bond through the radical rebound pathway (Hill, 1983).

A breakthrough of high selectivity was achieved in 2010, with manganese porphyrin complexes and sodium hypochlorite as the oxidant. Various hydrocarbon substrates were readily chlorinated, with only a trace amount of oxygenation products were (Liu & Groves, 2010). High regioselectivity and stereoselectivity were found, showing great variation in the C-H chlorination with hypochlorous acid. Later studies proved that the axial ligand was a key factor in controlling the lifetime of the carbon substrate radicals (Liu et al., 2012). This inspiring finding indicated that there would be a general strategy to biomimetically control and develop the C-H activation reactions through managing the radical rebound process.

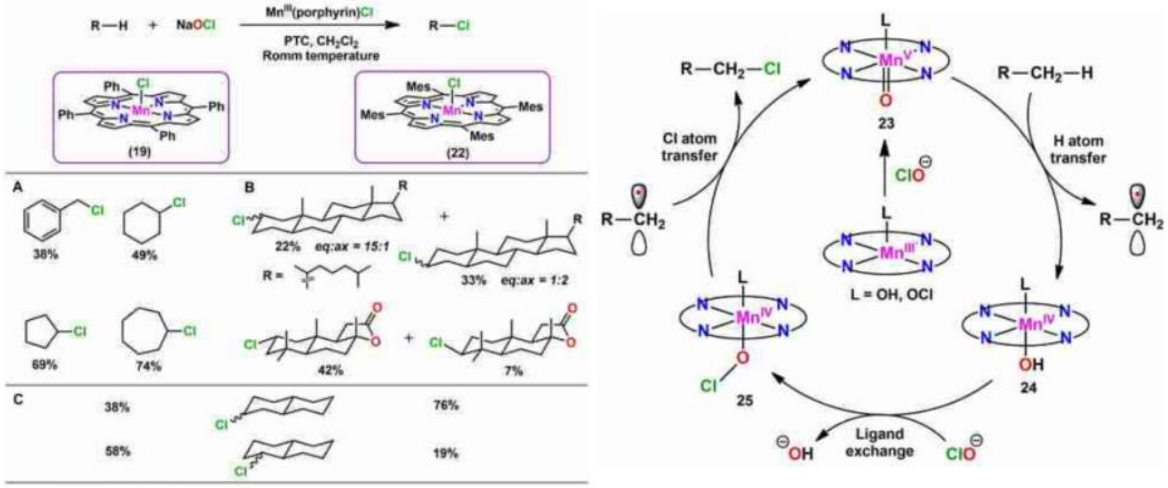

Fig. 2 Mechanism of C-H halogenation catalyzed by Mn^{III}(TPP)Cl

2.2.2 Heme-iron(III) complexes

The very first example studied of the heme-iron(III) complex family was the CYP450 of which the mechanism had been illustrated above. Yet CYP450 only utilizes the molecular oxygen on the heme-center to hydroxylate the substrates, and no halogenation capability was found so far. Later on, another family, chloroperoxidase(CPO), which had a similar structure to CYP450 was found to generate hypohalous acids for C-H halogenation. (Timmins & Visser, 2018).

The general mechanism of CPO is shown in the following scheme, which is similar to the 'radical rebound mechanism', but the *cpd II* does not interact selectively with the active sites of the substrate, only releases free diffusing hypohalous acids. At first, the ground state heme-iron(III) complex (A) is oxidized by H_2O_2 and forms hydroperoxo-intermediate (B), which results in *cpd I* (C) through the cleavage of peroxide O-O bond by Glu_{183}. A halide ion is then oxidized by c*pd I* (C) and forms the ferric-hypohalide intermediate (Fe-O-X, D). in the end, hypohalous acids are released and ground state heme-iron(III) complex (A) is regenerated by the addition of water. The hypohalous acids could activate a large variety of electron-rich substrates such as aromatic rings, but with low selectivity and stability. Therefore, CPO is barely applied in industrial chemistry and is less focused on its ramifications.

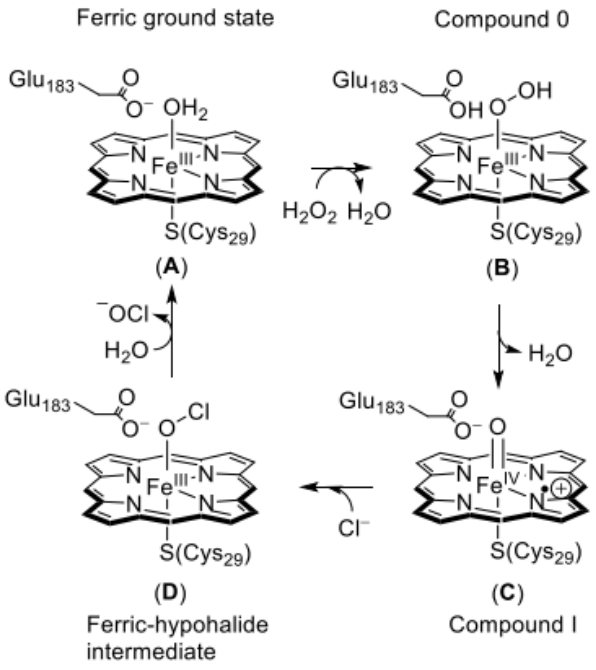

Fig. 3 Catalytic cycle of the heme haloperoxidase from chloroperoxidases (CPO).

2.2.3 Non-heme planar tetradentate iron complexes

Even though the C-H halogenation had been achieved by manganese porphyrin complexes, iron porphyrin complexes hadn't been revealed of such capability. Then the focus was put on heme-mimetic synthetic ligands. This study is inspired by and ameliorated previous studies conducted by Prof. Chow Stephen and coworkers of the Department of Science and Environmental Studies, EdUHK (Chang et al., N/A, not published). Although, as stated, non-heme iron(IV)-oxo-halide complexes had been reported continuously for C-H halogenation, non-heme iron(V)-oxo-halide species were barely reported. Chang and coworkers successfully synthesized the Fe^{III}(acacen)(Cl/Br) and Fe^{V}(acacen)(oxo)(Cl/Br) as the first known non-heme $iron^{V}$-oxo-halide complex with a planar tetradentate structure for sp^3 C-H bond halogenation (shown in figure 4). An excellent selectivity (>99%) was obtained in the halogenation of cyclohexane. It was proposed that with TFA(Trifluoroacetic acid), the iron(III) planar tetradentate halide complexes could be a potential platform for oxidative C-H bond activation and functionalization.

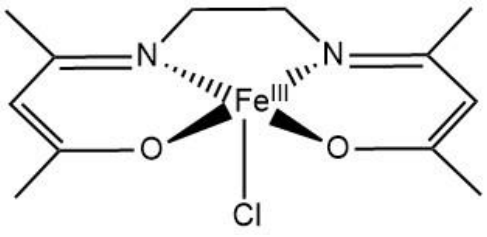

Fig. 4a Fe^{III}(acacen)Cl

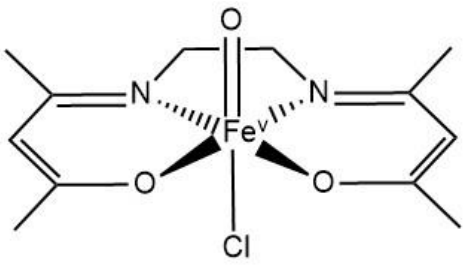

Fig. 4b Fe^{V}(acacen)(oxo)Cl

2.3 αKG dependent non-heme iron(II) models and its ramification for C-H activation

2.3.1 αKG dependent non-heme iron(II) hydroxylases and halogenases

CYP450 and its heme-iron cofactor were not the only catalytical system utilizing high-valent iron-oxo intermediates to activate C-H bonds. Another major example was the superfamily of α-ketoglutarate dependent non-heme $iron^{II}$ complex. In the αKG-Fe(II) systems, the iron center is coordinated by two facial histidines and one carboxylate, normally referred to as the '2-His-1-carboxylate facial triad' (Huang & Groves, 2017). The αKG-Fe(II) complexes could also perform both hydroxylation and halogenation of the C-H bond in the 'radical rebound mechanism' introduced above. Apart from the TauD as the dioxygenase, the syringomycin halogenase (SyrB2) is a typical specie of αKG-Fe(II) superfamily that selectively catalyze the C-H chlorination rather than hydroxylation.

2.3.2 Synthetic non-heme iron(II) halogenases

The utilization of natural enzymes was not favored in chemistry studies due to the strict requirement of the reaction condition and the higher complexity of the natural complexes. Thus based on the cis-coordinated iron(II) structure, researchers developed artificial complexes to simulate the αKG-Fe(II) complex.

The first model of this type of catalyst was reported by Que and co-workers, shown in figure 5 (Que Jr., 1993). However, the existence of $[Fe^{IV}(O)(TPA)(Cl)]^{+}$ could be only achieved in -

40°C condition and lasted for about 20s time, which was still not a satisfying performance(Rohde et al., 2006).

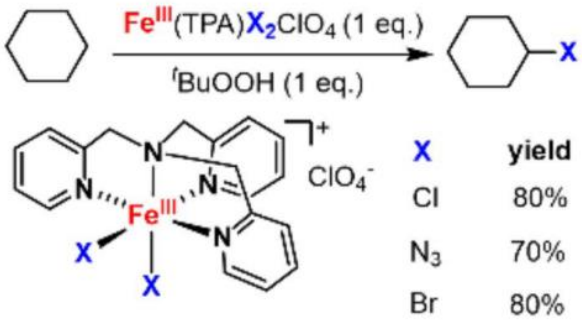

Fig. 5a [$FeCl_2$(TPA)]ClO_4

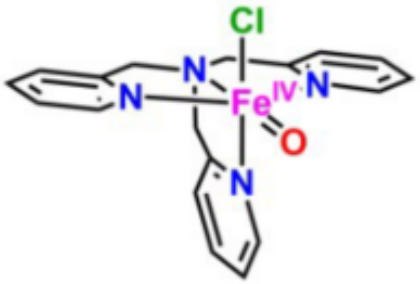

Fig. 5b [Fe^{IV}(O)(TPA)(Cl)]$^+$

After the start of Que's work, the development of the tetracoordinate tripodal topology iron complex had been continuously updated. In 2010, Comba and coworkers reported a well-defined functional halogenate model with a tetradentate bipyridine ligand system **L** (**L** = Me_2Py_2-DNDE, shown in figure 6a) with H_2O_2, TBHP, and PhIO as the oxidant (Comba & Wunderlich, 2010). Halogenation of TBHP as the oxidant to form compound I provided the highest efficiency, yet the selectivity of halogenation over hydroxylation was quite low (<1:1), while PhIO trials provided the highest selectivity (>10:1). The author interpreted the result based on computational studies that unwanted alkoxy radicals (O-tBu from TBHP) which led to a $[Fe^{IV}=O\ (OH_2)(L)]^{2+}$ precursor were responsible for the reduced selectivity. Hydrogen atom abstraction(HAA) was determined to be the rate-limiting step and preventing the oxygen-based radicals may efficiency of the future models(Comba & Wunderlich, 2010).

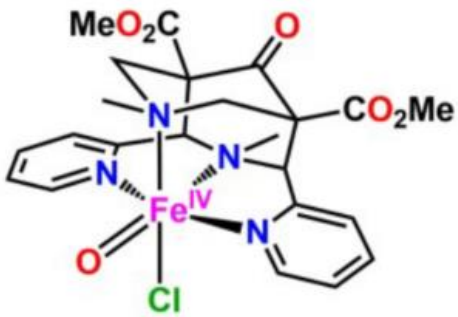

Fig. 6a [Fe^{IV}=O(Cl)(Me2Py2-DNDE)]

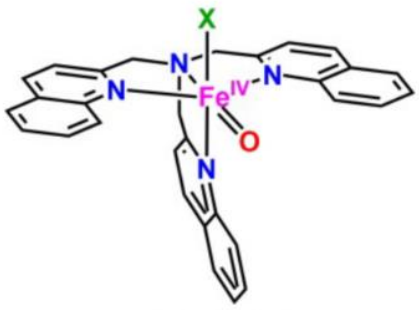

Fig. 6b [Fe^{IV}(O)(TQA)(Cl)]+ (X=Cl)

Later on, Que and coworkers published a high valent iron-oxo-halo complex which could exist at -40℃ for around 5mins (Puri et al., 2016). Addition of NBu_4Cl to $[Fe^{IV}(O)(TQA)(MeCN)]^{2+}$ in MeCN at -40 °C resulted in ligand exchange which formed an oxoiron(IV) complex $[Fe^{IV}(O)(TQA)(Cl)]^{+}$ (shown in figure 6b). This model showed high selectivity catalyzing the halogenation of cyclohexane but weaker selectivity to toluene. The author raised 2 possible pathways laid behind the results, the substrate radical may conduct a fast rebound with compound 1 after HAA; or the substrate radical may escape the solvent cage and react with other chemicals in the solution. They also concluded that the *S*=2 spin state is naturally preferred for the oxoiron(IV) oxidants in the halogenates and C-O bond formation between substrate radical and molecular oxygen is more rapid than C-Cl bond formation through the radical rebound mechanism (Puri et al., 2016).

2.4 Research gap

In general, natural catalytical systems including heme-metal complexes and αKG dependent iron complexes had both been revealed of their capability of C-H bond hydroxylation and halogenation. Meanwhile, the cis-coordinated model which is an artificial imitation of αKG dependent enzyme group had also shown a similar capability. However, selective C-H halogenation could only be achieved with heme-manganese complexes, but not heme-iron complexes. Thus, synthetic heme-mimetic models were raised to solve such problems. Besides, high-valent iron-oxo intermediate was extremely reactive at room temperature and open atmosphere. The formation of complexes with various ligands and models is believed to lower such reactivity for identification and research on the intermediates. Up till now, the heme-mimetic models (planar tetradentate iron complexes) were barely reported for C-H halogenation. And such a situation led to the research area of this project.

3. Methodology

3.1 Synthesis of the half-ligand

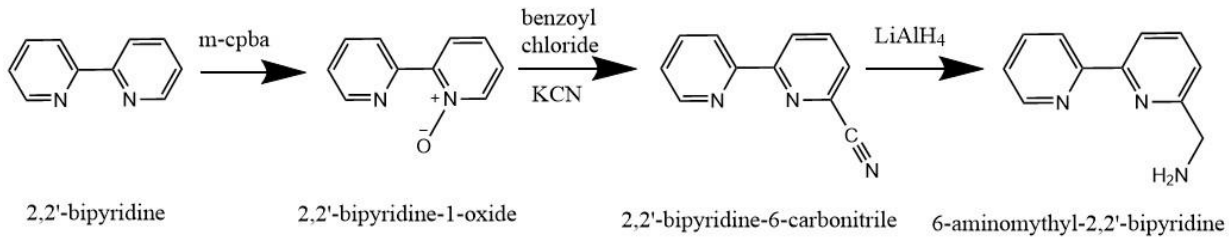

Fig. 7 reaction pathway of the half ligand.

2,2'-bipyridyl-N-oxide (2): A solution of 2,2'-bipyridine (10g, 64.0mmol) in 40mlL of $CHCl_3$ was stirred at a 0℃-ice bath for 40min. A solution of m-chloroperbenzoic acid (19g, 93.6mmol, purity 85%) in 150mL of $CHCl_3$ was added dropwise to the 2,2'-bipyridine solution over 80 min and the mixture was stirred at room temperature for 20h. The solution was washed with 5% aqueous Na_2CO_3 solution (100mLx3), dried with anhydrous $MgSO_4$, and concentrated with a rotary evaporator. The Na_2CO_3 washings were concentrated and extracted with $CHCl_3$ (70mLx4). The extract was dried with anhydrous $MgSO_4$ and concentrated. Each residual oil solution was combined and dissolved in ether. The undissolved 2,2'-bipyridine-N, N'-dioxide and side products were removed by filtration. The filtrate was filtrated with silica gel and flushed with ether to remove unreacted 2,2'-bipyridine. The 2,2'-bipyridyl-N-oxide was flushed out with DI water and concentrated. The residual oil was redissolved in ether and dried again with anhydrous $MgSO_4$, concentrated, and dried under vacuum overnight to obtain a yellowish solid (6.53g, 37.9mmol, yield 59.2%).

Spectra information: ^{1}H NMR ($CDCl_3$): 8.96, 8.69-8.82(2H), 8.11-8.26(2H), 7.70-7.94(1H), 7.29-7.36(3H). ATR-IR (cm^{-1}): 3070, 1582, 1492, 1444, 1417, 1250, 1033, 759, 720, 618,575.

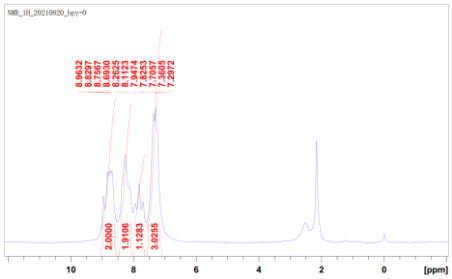

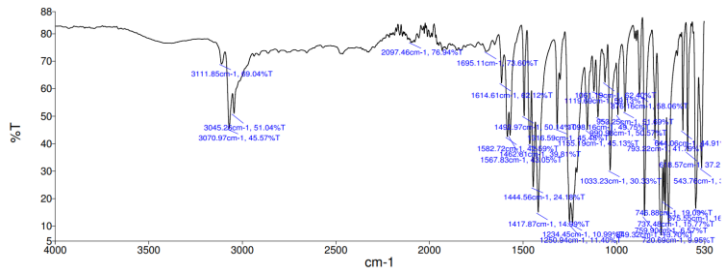

2,2'-bipyridine-6-carbonitrile (3): **2** (5.16g, 30mmol) was added to a solution of KCN (6.60g, 102mmol) in 40mL of DI water. The mixture was stirred to fully dissolve. Benzoyl chloride (7mL, 60mmol) was added dropwise over 20min to the stirred mixture. The mixture was stirred overnight at room temperature and extracted with EtOAc. The EtOAc solution was concentrated and chromatographed on a silica gel column, eluting with a mixture of petroleum ether and EtOAc (5:1). The second fraction of eluate was collected, dried with anhydrous $MgSO_4$, and concentrated to obtain an orange-yellow solid (1.9g, 10.5mmol, yield 35%).

Spectra information: ^{1}H NMR ($CDCl_3$): 8.64, 8.42, 7.96, 7.85, 7.75, 7.46. ATR-IR (cm^{-1}): 3064.37, 2237.91, 1582.05, 1558.11, 1454.74, 1429.48, 1266.51, 1084.51, 1045.21, 988.33, 775.84. HRMS(ESI) found *m/z* 182.06915$[M+H]^+$, $C_{11}H_8N_3$ requires *m/z* 182.07127. Mp: 118-120℃.

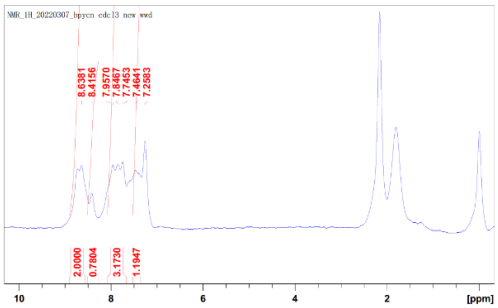

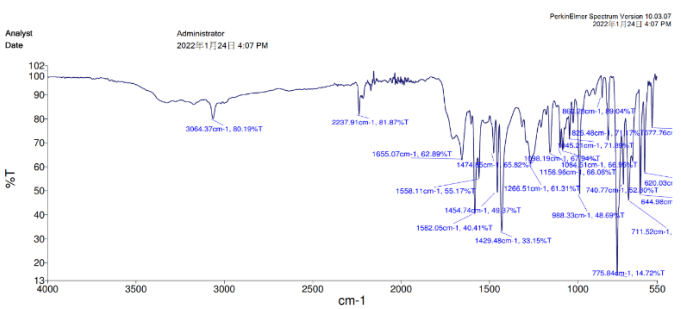

6-(Aminomethyl)-2,2'-bipyridine (4): A solution of **3** (1g, 5.5mmol) in 10ml anhydrous ether was added dropwise over 10min into a stirring suspension of $LiAlH_4$ (0.6g, 15.7mmol) in 30mL anhydrous ether. The mixture was stirred and reflexed for 30min, cooled down in an ice bath after the reaction. 10mL of DI water was added dropwise followed by 5mL 10%

aqueous NaOH solution. The mixture was filtrated, and the filtrate was washed with ether. The ether solution was dried with anhydrous $MgSO_4$ and concentrated to give the product a deep orange sticky oil (0.8g, 4.5mmol, yield 81%).

Spectra information: ^1H NMR ($CDCl_3$): 1.25, 4.05, 7.26, 7.78, 8.22, 8.39, 8.64. ATR-IR (cm^{-1}): 3306.05, 2060.56, 1582.82, 1563.43, 1455.44, 1430.33, 1092.95, 1042.11, 992.92, 760.74. HRMS(ESI) found *m/z* 186.10066 $[M+H]^+$, $C_{11}H_{12}N_3$ requires *m/z* 186.10257.

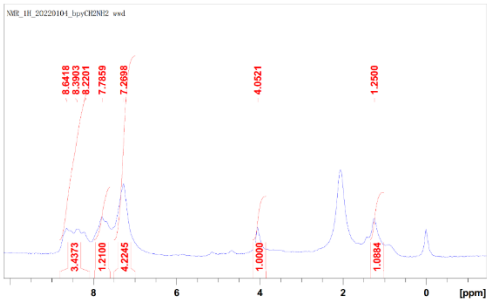

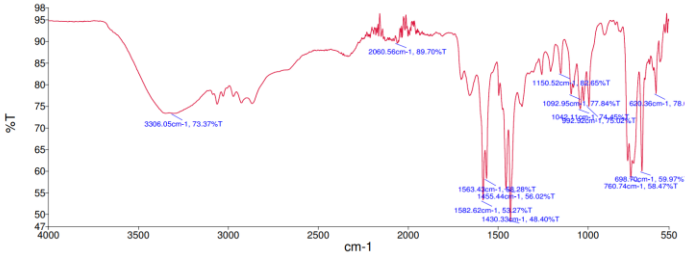

3.2 Synthesis of iron complexes

[Fe(N-bmpm)(Cl)]Cl, (1-Cl): **1-Cl** was synthesized through the one-pot method. **4** (0.01g, 0.054mmol), 2-Pyridinecarboxaldehyde (0.006g, 0.054mmol), $FeCl_3$ (0.01g, 0.06mmol) and Triethylamine (0.006g, 0.06mmol) were dissolved in 2mL methanol. The mixture was heated and stirred at 55℃ for 2h. After cooled down to room temperature, the clear brownish-purple reaction mixture was recrystallized with ether and washed with ether. The purple powder was redissolved in acetone and filtered. The clear purple solution was then concentrated and dried under vacuum to collect purple solid (0.0182g, 0.049mmol, 90%). *(N-bmpm = *(E)*-N-([2,2'-bipyridin]-6-ylmethyl)-1-(pyridin-2-yl) methanimine)

Spectra information: HRMS(ESI) found *m/z* 365.02066 $[M-Cl]^+$, $C_{17}H_{14}N_4FeCl$ $[M-Cl]^+$ calcd. to be 365.02564.

[Fe(N-bmop)(Cl)]Cl, (2-Cl): 2-Cl was synthesized separately. A solution of acetylacetone (0.015g, 0.15mmol) in 1mL CH_2Cl_2 was added dropwise to a stirring solution of **4** (0.024g, 0.128mmol) in 1mL CH_2Cl_2. Anhydrous $MgSO_4$ (0.2g, 1.5mmol) was added for dehydration.

The mixture was stirred at room temperature for 2h and filtered. The solution was extracted with 1M aqueous acetic acid solution to remove unreacted **4**, dried with anhydrous $MgSO_4$, and then concentrated. The residue oil was redissolved in 2mL MeOH to synthesize the complex.

$FeCl_3$ (0.024g, 0.15mmol) and Triethylamine (0.015g, 0.15mmol) was added to the residue oil solution. The mixture was heated and stirred at 60℃ for 2h. After cooled down to room temperature, the turbid brown liquid was recrystallized with ether, resulting in a deep orange solution and brown precipitate. The brown solid was redissolved in acetone and filtered. The acetone solution was then concentrated and dried under vacuum to give a brown solid (0.022g, 0.062mmol, 50%). *(N-bmop = *(2E,3Z)-N*-([2,2'-bipyridin]-6-ylmethyl)-4-(oxidaneyl)pent-3-en-2-imine)

Spectra information: HRMS(ESI) found *m/z* 357.02707 $[M-Cl]^+$, $C_{16}H_{16}N_3OFeCl$ $[M-Cl]^+$ calcd. To be 357.03313.

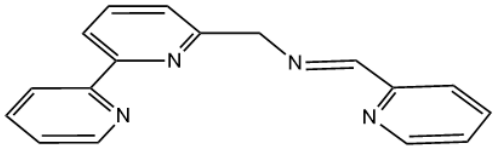

(*E*)-*N*-([2,2'-bipyridin]-6-ylmethyl)-1-(pyridin-2-yl)methanimine

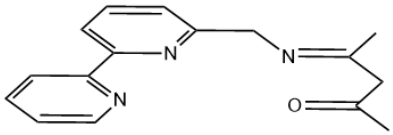

(*E*)-4-(([2,2'-bipyridin]-6-ylmethyl)imino)pentan-2-one

3.3 Catalytical halogenation of aliphatic C-H bond

	10^{-3}M iron complex		1M H_2O_2	Cyclohexane	1M TFA	1M TBACl	ACN
1	**1^{II}-Cl**	2 mL	100 μL	65 μL	-	-	200 μL
2	**1^{II}-Cl**	2 mL	100 μL	65 μL	100 μL	-	100 μL
3	**1^{II}-Cl**	2 mL	100 μL	65 μL	100 μL	100 μL	-
4	**2^{III}-Cl**	2 mL	100 μL	65 μL	-	-	200 μL
5	**2^{III}-Cl**	2 mL	100 μL	65 μL	100 μL	-	100 μL

6	**2^{III}-Cl**	2 mL	100 μL	65 μL	100 μL	100 μL	-

(all the reactants were dissolved in ACN, 200μL 1M internal standard naphthalene was added)

One control group and two experimental groups were set for each iron complex. The reaction mixture of each group was stirred at 25℃ for 20h in the open atmosphere and then quenched with 200 μL 1M NaOH. The quenched mixture was then run over a short silica column to remove the metal complex before being examined with GC-MS.

3.4 Calibration curve of products/naphthalene

Naphthalene was added as the internal standard in the catalytical reaction to calculate the yields and selectivity. CAN solution of cyclohexanol, cyclohexanone, naphthelene was prepared with a certain concentration gradient (shown in the following table), and ran GC-MS.

	cyclohexanol	cyclohexanone	naphthalene		chlorocyclehexane	naphthalene
1	0.05 mM	0.05 mM	5 mM			
2	0.1 mM	0.1 mM	5 mM		0.1 mM	5 mM
3	0.2 mM	0.2 mM	5 mM		0.2 mM	5 mM
4	0.5 mM	0.5 mM	5 mM		0.5 mM	5 mM
5	1 mM	1 mM	5 mM		1 mM	5 mM
6	1.5 mM	1.5 mM	5 mM			

The ratio of integration area (counts*min), cyclohexanol to naphthelene and cyclohexanone to naphthelene, was plotted against the concentration of cyclohexanol and cyclohexanone. Equations were generated from the two separate graphs through linear regression analysis, shown as follows. Thus, the concentration of the products could be achieved.

Similar method was adopted to generate calibration curve of chlorocyclehexane, but only with less groups.

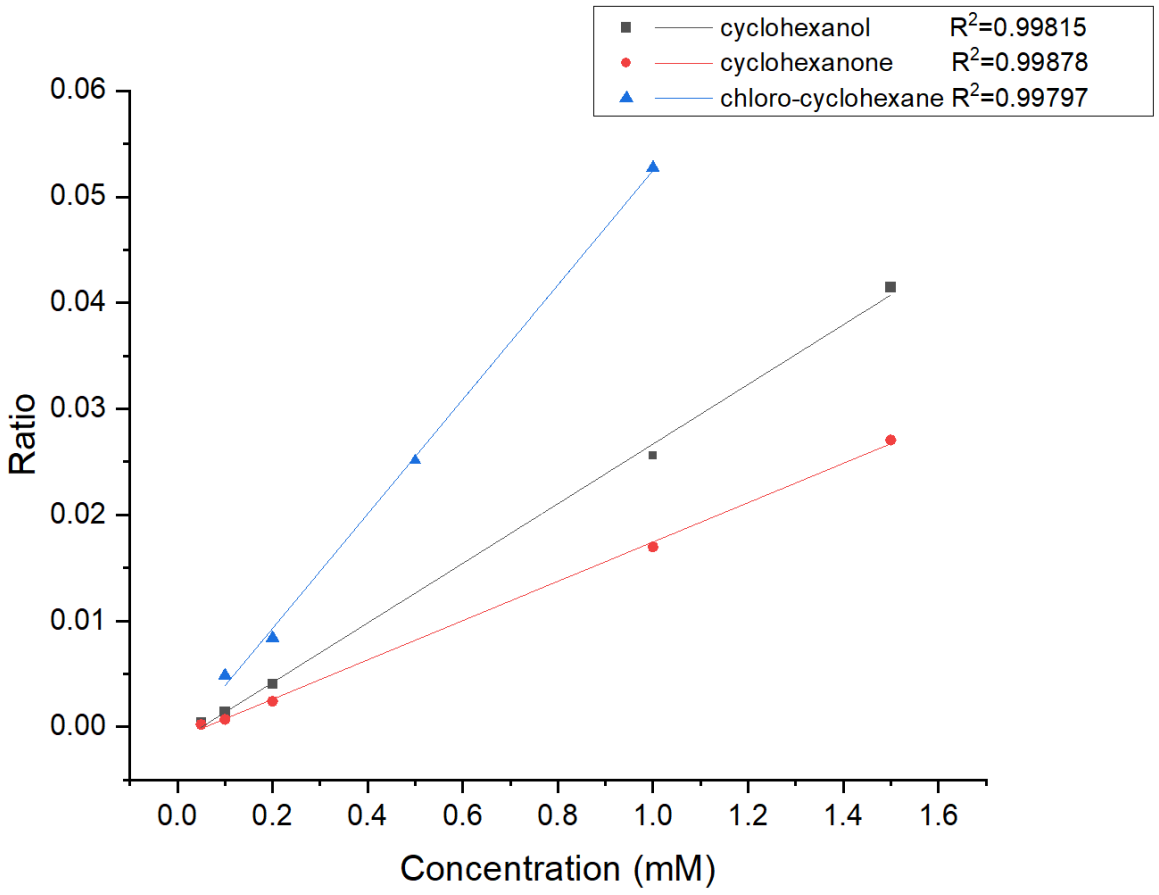

3.5 Analytical instrumentation

H-NMR: Proton nuclear magnetic resonance (^{1}H-NMR) spectroscopy is based on the phenomenon of NMR which could deduce the structure of the sample molecule. The spectrum is formed by different chemical shifts regarding the ^{1}H nuclei(a proton) as it is sensitive to the hybridization status. Thus the relative ratio of 1H nuclei in different states could be obtained (Günther, 2013).

GCMS: Mass spectrometry (MS) is a widely applied analytical technique that could measure the mass of a specific analyte within a sample. In an MS measurement, the analyte molecules are first introduced into an ionization source, then the MS system will generate and record signals when the ions reach the detector(Chen et al., 2019). The signals generated from different species in the sample are sorted by the mass-to-charge (*m/z*)ratios.

In GCMS (Gas Chromatography-Mass Spectrometry), the sample will be injected into a packed capillary column (stationary phase) by a steam of carrier gas (mobile phase, normally inert gas). Due to the ability of distribution between the mobile and stationary phases of each species in the sample being different, the sample could be separated according to the exit time (Harvey, 2000). Then the MS could generate the *m/z* ratio signals for separated chemicals.

HRMS(ESI): High-resolution mass spectrometry is a useful tool for analyzing complex sample matrices. The increased resolution of HRMS instrumentation makes it possible to separate peaks of compounds with close *m/z* and measure their *m/z* with standard 1 ppm accuracy. It is also used to distinguish isotopic distributions and generate fragmentation patterns, which improves the accuracy of chemical formula prediction (Beauchamp, Davis, & Pleil, 2020).

IR: Infrared absorbance spectroscopy is used to identify the analyte's chemical bonds and functional groups. The chemical bonds of the analyte vibrate at certain frequencies and could absorb the corresponding infrared lights with the same frequencies. An IR spectrum can be visualized in a graph of infrared light absorbance on the vertical axis vs. frequency or wavelength on the horizontal axis.

UV-vis: Ultraviolet-visible spectroscopy is used for quantitative analysis of the iron center of the catalyst. The spectrum will also reflect the visible color of the catalyst. Electrons in the coordination bond or non-bonding electrons could absorb energy from the ultraviolet or visible light and be excited to higher anti-bonding molecular orbitals. The energy absorbed by the transition of electrons would be recorded by the spectrometer and plotted in the spectrum of absorbance (A) versus wavelength (λ)(Mehta, 2011).

4. Results and discussion

4.1 Identification of ligand and precursors

2,2'-bipyridyl-N-oxide (2):

The IR spectrum of **2** had a general agreement with the previous study as shown in the following table:

Previous study	3394, 3060, **1582**, 1463, 1442, 1415, 1250, 1033, 849, 768, 720, 617,575.
This study	3070, **1582**, 1492, 1444, 1417, 1250, 1033, 759, 720, 618,575.

(Kodama, 2013).

Among these, the absorption peak at 1582cm^{-1} of the IR graph indicated the successful oxidation and the formation of the N-O bond. However, this could not exclude the existence of the side product 2,2'-bipyridyl-N'N-dioxide, which would show a similar pattern in the IR spectrum, due to the existence of the N-O bond.

The ^{1}H NMR spectrum of starting material 2,2'-bipyridine and side product 2,2'-bipyridyl-N'N-dioxide should show an equal proportion (2:2:2:2) since in these two compounds, hydrogen atoms were distributed symmetrically (shown in figure 8a). Whereas due to the abstraction of oxo-group on only the onside of the product molecule, the ^{1}H NMR spectrum of 2,2'-bipyridyl-N-oxide showed an obvious excursion and ratio turned to 2:2:1:3, which clearly differentiated the product from the starting material and side product. This ratio was also agreed with computational simulation (shown in figure 8b).

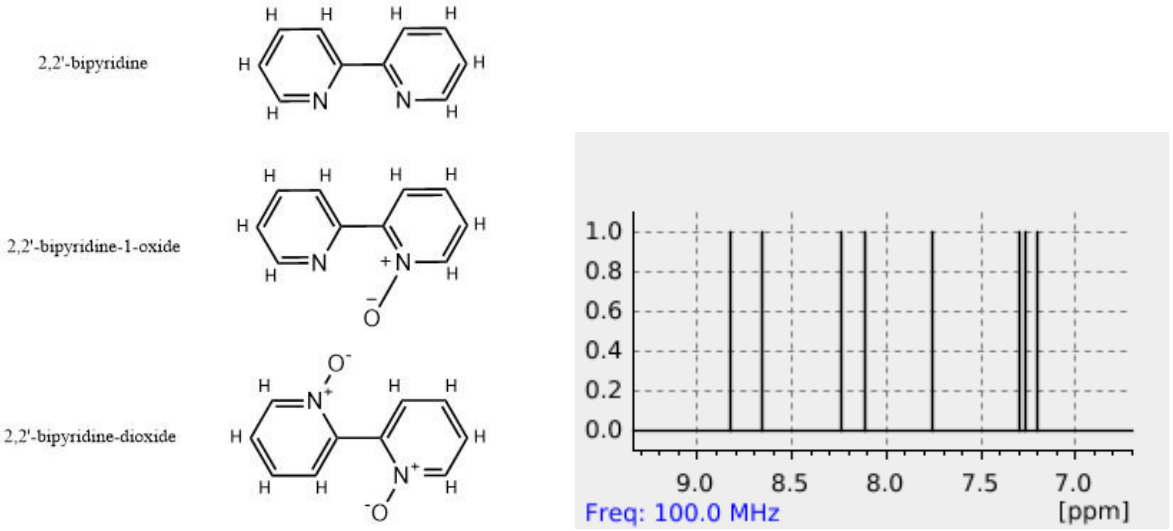

Fig. 8a Structural comparation of 2,2'-bipyridine, 2,2'-bipyridyl-N-oxide and 2,2'-bipyridyl-N'N-dioxide.

Fig. 8b Computational simulation of the ^{1}H-NMR spectrum of 2,2'-bipyridyl-N-oxide

Focusing on the chemical shifts, the ^{1}H NMR spectrum of the product was compared to the previous studies and the chemical shifts and hydrogen ratio (2:2:1:3) were generally agreed upon.

Previous study 1	8.93(1H), 8.75(1H)	8.12-8.42(2H)	7.85(1H)	7.18-7.50(3H)
Previous study 2	8.90(1H),8.74(1H)	8.32(1H)	7.84 (1H)	7.40-7.33(2H), 7.27 (1H)
This study	8.96/8.69-8.82(2H)	8.11-8.26(2H)	7.70-7.94(1H)	7.29-7.36(3H)

(David, 1982; Kodama, 2013).

2,2'-bipyridine-6-carbonitrile (3):

The HRMS(ESI) confirmed the chemical formula as $C_{11}H_8N_3$. The IR spectrum of **3** had a general agreement with the previous study as shown in the following table:

Previous study	3063, 2924, **2236**, 1580, 1557, 1454, 1084, 1041
This study	3064, **2238**, 1582, 1558, 1455, 1429, 1267, 1085, 1045, 988, 776.

(Elbert et al., 2017).

The absorption peak at 2237cm^{-1} of the IR spectrum indicated the existence of the C≡N bond, the cyanide group, in the product. There was only one point in the TLC plate, which proved the purity of the product. However, the possibility to be the side product 2,2'-bipyridine-4-carbonitrile, which was the isomer of the expected product, was not excluded.

The ^{1}H NMR spectrum of the product was compared with the previous study, as well as the side product 2,2'-bipyridine-4-carbonitrile.

Previous study	8.68 (2H)	8.47 (1H)	7.96(1H), 7.87 (1H), 7.75 (1H)	7.39(1H)
This study	8.64 (2H)	8.42 (1H)	7.96/7.85/7.75 (3H)	7.46(1H)

(Elbert et al., 2017).

The chemical shifts of the spectrum found and that in the previous study showed high similarity, while both spectra showed a 2:1:3:1 ratio as seen in the table. In the contrast, for the isomer 2,2'-bipyridine-4-carbonitrile, there should be an 8.83 (1H) peak in ^{1}H NMR ($CDCl_3$), and the H-distribution should be in a 1:2:3:1 ratio.

Another proof of differentiation was the melting point. According to the previous study, the melting point of 2,2'-bipyridine-4-carbonitrile is 86℃ (Duric, 2011), whereas 125℃ for 2,2'-bipyridine-6-carbonitrile (Liao, 2014). The melting point of the product was found to be 118-120℃, indicating the product was 2,2'-bipyridine-6-carbonitrile. The lowered melting point might result from the wetness of the product.

6-(Aminomethyl)-2,2'-bipyridine (4):

The absorption peak at 3306cm^{-1} of the IR graph indicated the existence of the N-H bond (aliphatic primary amine) in the product. The disappearance of 2237cm^{-1}(C≡N bond, the cyanide group) indicated the reduction was successful, the cyanide group was reduced to the amino group. The rest of the IR graph showed a general similarity with **3** which means the bipyridine main structure was not influenced. The chemical shifts at 1.25 and 4.05ppm in the ^{1}H NMR graph showed the existence of hydrogen in -CH_2- and -NH_2. In accordance with the

previous study, the product would have a 4.61ppm shift with D_2O as solvent. As there was no D_2O temporarily in the lab, the 1.25ppm and 4.05ppm shifts in $CDCl_3$ were seen as acceptable proof for the product. The HRMS(ESI) also confirmed that the chemical formula is $C_{11}H_{11}N_3$.

4.2 Identification of the iron complexes

Fe^{II} (N-bmpm)(Cl), (1^{II}-Cl):

HRMS had confirmed the chemical formula to be $C_{17}H_{14}N_4FeCl$, while the isotope distribution pattern agreed with the computational simulation (shown in figure 9) that a chemical with an iron and a chloride should possess a high-low-medium pattern. The 1 m/z step size indicated that the complex has an overall 1 positive charge. In consideration of the ligand should be neutral with 0 charges and one chloride has 1 negative charge, the iron center in the complex form actually has 2 positive charges which mean the $iron^{III}$ chloride used was reduced to $iron^{II}$ and formed $iron^{II}$ complex. The reduction was possibly caused by the TEA used as the catalyst. Previous studies had reported the reduction ability of TEA (Schmallegger & Gescheidt, 2018).

The stereo structure of the complex could not be determined from the HRMS that whether **1^{II}-Cl** is cis or trans coordinated by the ligand. Up to the submission of this report, not enough crystal was grown for X-ray scattering. The atomic model remained to be revealed in further studies.

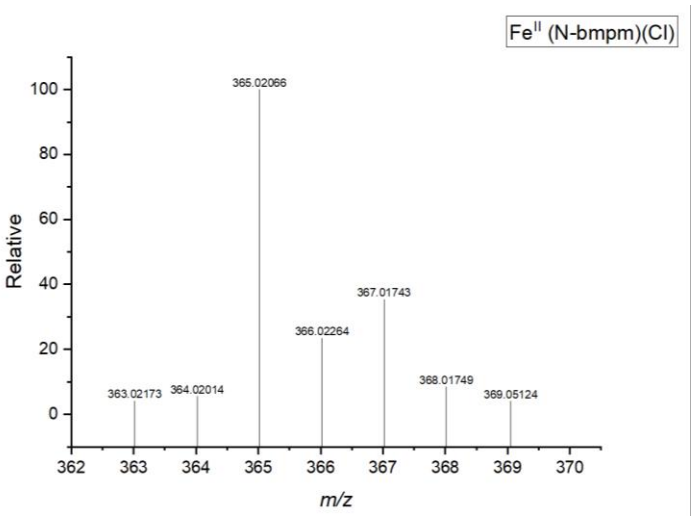

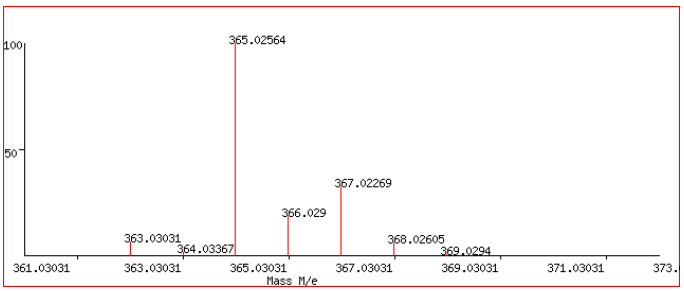

Fig. 9 Computational simulated HRMS of $C_{17}H_{14}N_4FeCl$

Fe^{III} (N-bmop)(Cl), (2^{III}-Cl):

HRMS had confirmed the chemical formula to be $C_{16}H_{16}N_3OFeCl$, while the isotope distribution pattern agreed with the computational simulation (shown in figure 10) that a chemical with an iron and a chloride should possess a high-low-medium pattern. The 1 m/z step size indicated that the complex has an overall 1 positive charge. In consideration of the ligand having 1 negative charge and one chloride ion having 1 negative charge, the iron center should be $iron^{III}$, which is different from complex **1^{II}-Cl**.

The stereo structure of the complex could not be determined from the HRMS that whether **2^{III}-Cl** is cis or trans coordinated by the ligand. Up to the submission of this report, not enough crystal was grown for X-ray scattering. The atomic model remained to be revealed in further studies.

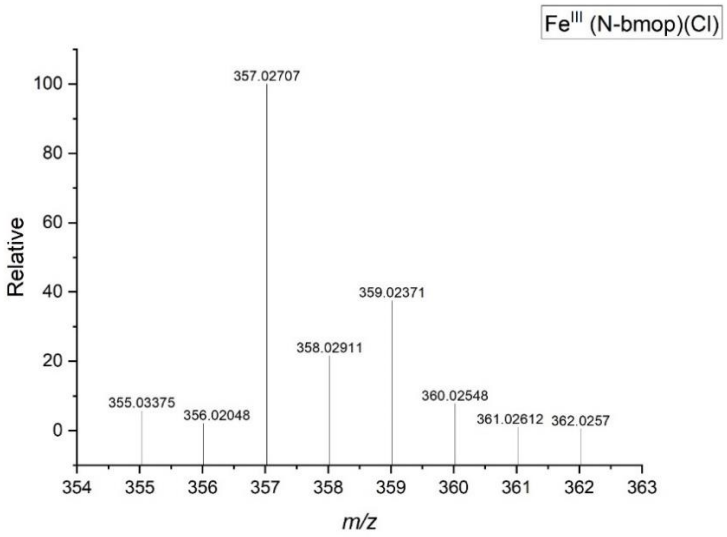

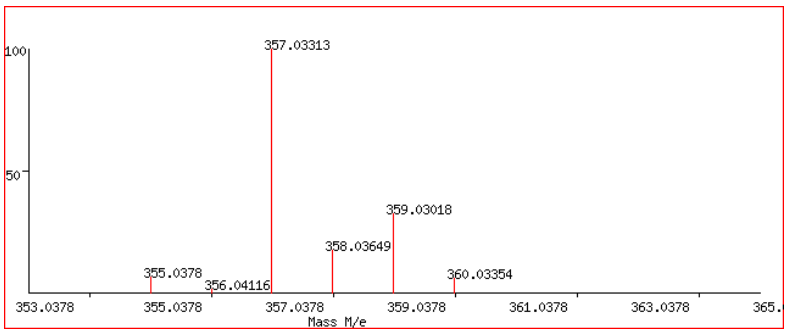

Fig. 10 Computational simulated HRMS of $C_{16}H_{16}N_3OFeCl$

4.3 Examining the formation of high-valent iron-oxo intermediate

3mL (10^{-3}M) **1^{II}-Cl** was oxidized by adding 150μL (1M) H_2O_2 and 150μL (1M) acetic acid (50equiv.). Uv-vis spectra were generated at 200-1000nm with a 1min interval for 60min. The $iron^{II}$ absorption peak at 530nm was found to decrease with time, which indicated a successful reaction of **1^{II}-Cl** with H_2O_2. However, no peak increased with time which indicated that the formation of the high-valent iron-oxo complex could not be determined with current observation. After 24h, the 530nm peak did not reverse to the original absorbance. The same treatment was performed on **2^{III}-Cl** and a similar observation was found in the oxidation of **2^{III}-Cl** with 50equiv. H_2O_2.

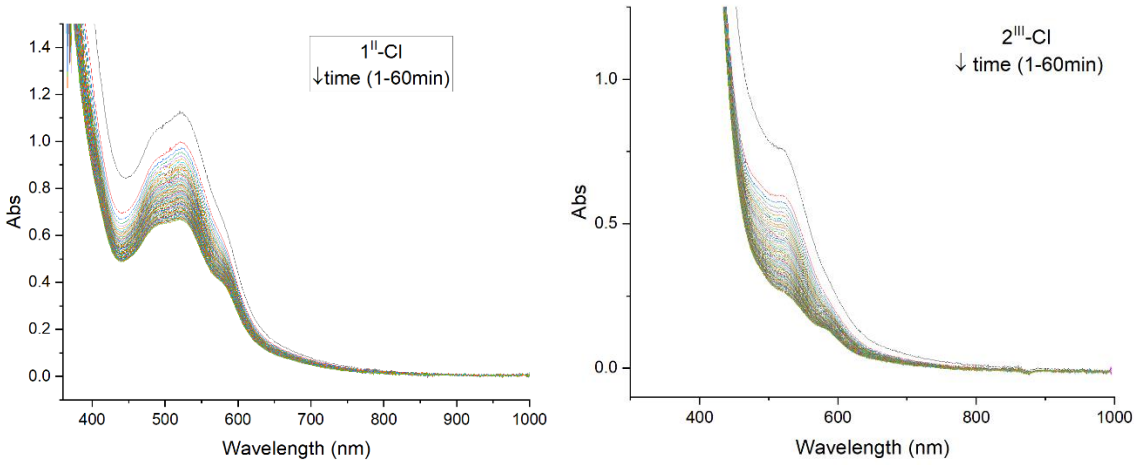

4.4 Catalytical performance of the complexes

	Reaction mixture			Yield			Total yield	Selectivity ($C_6H_{11}Cl$)	Total TON
		Acicd	Additive	$C_6H_{11}Cl$	$C_6H_{11}OH$	$C_6H_{10}O$			
1	**1^{II}-Cl** + H_2O_2 + Cyclohexane	-	-	0%	2.56%	0%	2.56%	0%	0.38
2		TFA	-	0.16%	13.10%	7.28%	20.54%	0.78%	3.08
3		TFA	TBACl	0.12%	2.33%	2.84%	5.28%	2.20%	0.79
4	**2^{III}-Cl** + H_2O_2 + Cyclohexane	-	-	0%	6.02%	0%	6.02%	0%	0.90
5		TFA	-	0.75%	9.57%	5.95%	16.28%	4.63%	2.44
6		TFA	TBACl	0.26%	2.34%	3.94%	6.54%	3.94%	0.98

The yield was calculated according to the calibration curve of products and naphthalene.

It could be found that the halogenation product only appeared with the existence of TFA, while the effect of TBACl varied in two complexes. With the addition of TBACl the selectivity of halogenation increased for **1^{II}-Cl**, but decreased **2^{III}-Cl**. Meanwhile, TBACl was found to inhibit the catalytical reaction of **1^{II}-Cl** and **2^{III}-Cl**, as the total yield decreased 60%-70% with the existence of TBACl.

Generally speaking, the selectivity and efficiency were not satisfying. The iron complexes may act not as a catalyst since the total TON was less than 1 in trial 1, 3, 4 and 6. Even in trial 2 and 5, the total TON was only in single-digit level, which indicated a poor catalytical ability. The low TON was also agreed with the observation in ***4.3***, that the iron-center absorbance peak could not reverse after adding H_2O_2.

5. Limitation

Synthetic procedure: The first influential factor in the accuracy of the first part of this study was the resonance frequency of the ^{1}H-NMR used in the laboratory. Compared with wildly used 400 MHz, the 60 MHz ^{1}H-NMR had a limited differentiation power to generate sharp and narrow peaks of ^{1}H chemical shift. As it could be found above, the ^{1}H-NMR spectra attached in this study had overlapping peaks and thus influenced the reliability of the ligand identification. Thus the identification of each compound had to rely on a combination of information from various methods but not accurately by chemical shifts and integration.

Another unsatisfactory aspect was the comparatively lower yield in the first few steps. Due to the unversed performance of mine when carrying out the reaction and purification, the yield of each reaction could not reach as reported. Thus it was kind of wasting the materials and more time was spent in this stage than expected.

As stated, the schedule was not followed tightly as expected and the time left for examining the catalytical performance of the complexes was truly tight. As a result, several further questions had to be left to further studies.

Complex identification and catalytical performance: Firstly, more information is needed to better study the iron complexes formed in this study. From the HR-MS(ESI), only the chemical formula could be assured and the stereo-structure still remained unknown, whether the complex was heme-like planar tetradentate or αKG-Fe(II)-like cis-coordinated structure. Meanwhile, the UV spectra after adding oxidants could not prove the formation of a high-valent intermediate, but only the complex could be oxidized. The resulting mixture also did not show a reverse from the oxidized product to the original complex, which was not an expected observation of a capable catalyst in the C-H bond activation.

Even though halogenation products were found in the catalytical reactions of both complexes with the existence of TFA or TFA/TBACl, both complexes did not show high efficiency and

selectivity as expected. One deficiency was that the scale of the reaction was only at 10^{-3}M level, which was much lower than previous studies. Another factor that may lead to the offset of the results was that the internal standard used to generate the calibration curve was too high in concentration. Thus, the scale of the integrated area ratio in GC-MS was too low, and led to a decreased accuracy.

Insights on further studies: The reduction of 2,2'-bipyridine-6-carbonitrile with $LiAlH_4$ to synthesize 6-(aminomethyl)-2,2'-bipyridine(**4**) was rarely reported in the previous studies. This method provided a satisfactory yield and fewer side-product and could be applied to facilitate further studies. Apart from the two complexes formed in this study, there are still various kinds of ligands that could be generated from the half-ligand, **4**. For example, **4** could be used in the following reactions of complex formation in further studies. Meanwhile, the stereochemical structure of different iron complexes is left to be determined in further studies, when a satisfactory single crystal was grown for X-ray scattering.

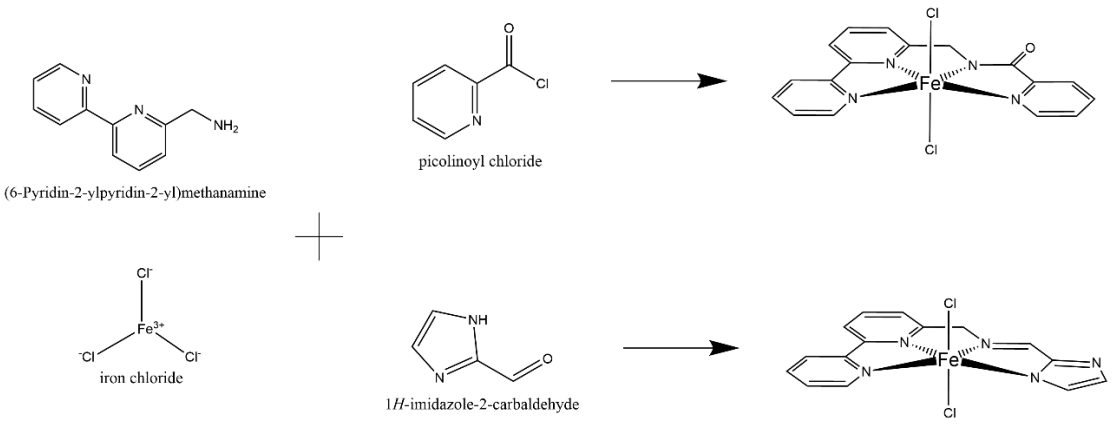

Moreover, the catalytical performance of iron complexes has high relevance to the reaction condition, and it requires persistent temptations to acquire an optimal condition. Due to the time limitation, optimizing the catalytical performance is left to further studies.

6. Conclusion

In summary, this study had two major achievements. The half-ligand, 6-(aminomethyl)-2,2'-bipyridine (**4**) was successfully synthesized and identified. Then, two iron complexes were generated based on the half-ligand **4** and assured with their chemical formula through HR-MS(ESI). What's more, the iron complexes formed in this study had shown the capability of C-H bond activation, including both hydroxylation and halogenation. The results generally solved the problems raised but did not fulfill the expectations of efficiency and selectivity.

References

Bullock, M. W., Hand, J. J., & Stokstad, E. R. (1956). Syntheses of 6-substituted purines. *Journal of the American Chemical Society*, *78*(15), 3693-3696.

Chen, T., Yao, Q., Nasaruddin, R. R., & Xie, J. (2019). Electrospray Ionization Mass Spectrometry: A Powerful Platform for Noble-Metal Nanocluster Analysis. *Angewandte Chemie (International Ed. In English)*, *58*(35), 11967–11977. https://doi.org/10.1002/aSnie.201901970

Comba, P., & Wunderlich, S. (2010). Iron-Catalyzed Halogenation of Alkanes: Modeling of Nonheme Halogenases by Experiment and DFT Calculations. *Chemistry–A European Journal*, *16*(24), 7293-7299.

Davis, C., Pleil, J., & Beauchamp, J. (Eds.). (2020). Breathborne biomarkers and the human volatilome.

Elbert, B. L., Farley, A. J., Gorman, T. W., Johnson, T. C., Genicot, C., Lallemand, B., ... & Dixon, D. J. (2017). C− H cyanation of 6-ring N-containing heteroaromatics. *Chemistry–A European Journal*, *23*(59), 14733-14737.

Groves, J. T., Kruper Jr, W. J., & Haushalter, R. C. (1980). Hydrocarbon oxidations with oxometalloporphinates. Isolation and reactions of a (porphinato) manganese (V) complex. *Journal of the American Chemical Society*, *102*(20), 6375-6377.

Günther, H. (2013). *NMR spectroscopy: basic principles, concepts and applications in chemistry*. John Wiley & Sons.

Harvey, D. (2000). *Modern analytical chemistry* (Vol. 1). New York: McGraw-Hill.

Hausinger, R. P. (2004). Fe (II)/α-ketoglutarate-dependent hydroxylases and related enzymes. *Critical reviews in biochemistry and molecular biology*, *39*(1), 21-68.

Hill, C. L., Smegal, J. A., & Henly, T. J. (1983). Catalytic replacement of unactivated alkane carbon-hydrogen bonds with carbon-X bonds (X= nitrogen, oxygen, chlorine, bromine, or iodine). Coupling of intermolecular hydrocarbon activation by MnIIITPPX complexes with phase-transfer catalysis. *The Journal of Organic Chemistry*, *48*(19), 3277-3281.

Huang, X., & Groves, J. T. (2017). Beyond ferryl-mediated hydroxylation: 40 years of the rebound mechanism and C–H activation. *JBIC Journal of Biological Inorganic Chemistry*, *22*(2), 185-207.

Kodama, K., Kobayashi, A., & Hirose, T. (2013). Synthesis and spectral properties of ruthenium(II) complexes based on 2,2′-bipyridines modified by a perylene chromophore. *Tetrahedron Letters*, *54*(40), 5514–5517. https://doi.org/10.1016/j.tetlet.2013.07.150

Liu, W., & Groves, J. T. (2010). Manganese porphyrins catalyze selective C− H bond halogenations. *Journal of the American Chemical Society*, *132*(37), 12847-12849.

Liu, W., Huang, X., Cheng, M. J., Nielsen, R. J., Goddard III, W. A., & Groves, J. T. (2012). Oxidative aliphatic CH fluorination with fluoride ion catalyzed by a manganese porphyrin. *Science*, *337*(6100), 1322-1325.

Mehta, A. (2011). Ultraviolet-Visible (UV-Vis) Spectroscopy–Principle. *Pharma XChange*, *13*, 12.

Morimoto, Y., Shimaoka, Y., Ishimizu, Y., Fujii, H., & Itoh, S. (2019). Direct Observation of Primary C− H Bond Oxidation by an Oxido-Iron (IV) Porphyrin π-Radical Cation Complex in a Fluorinated Carbon Solvent. *Angewandte Chemie International Edition*, *58*(32), 10863-10866.

Puri, M., Biswas, A. N., Fan, R., Guo, Y., & Que, L. (2016). Modeling Non-Heme Iron Halogenases: High-Spin Oxoiron(IV)-Halide Complexes That Halogenate C-H Bonds. *Journal of the American Chemical Society*, *138*(8), 2484–2487. https://doi.org/10.1021/jacs.5b11511

Que Jr. (1993). Alkane functionalization at nonheme iron centers. Stoichiometric transfer of metal-bound ligands to alkane.

Rohde, J. U., Stubna, A., Bominaar, E. L., Münck, E., Nam, W., & Que, L. (2006). Nonheme oxoiron (IV) complexes of tris (2-pyridylmethyl) amine with cis-monoanionic ligands. Inorganic chemistry, 45(16), 6435-6445.

Schmallegger, M., & Gescheidt, G. (2018). Benzil/triethylamine: a photo-reducing system for Cu2+. *Monatshefte für Chemie-Chemical Monthly*, *149*(3), 499-504.

Srnec, M., & Solomon, E. I. (2017). Frontier Molecular Orbital Contributions to Chlorination versus Hydroxylation Selectivity in the Non-Heme Iron Halogenase SyrB2. *Journal of the American Chemical Society*, *139*(6), 2396–2407. https://doi.org/10.1021/jacs.6b11995

Timmins, A., & Visser, S. P. de (2018). A Comparative Review on the Catalytic Mechanism of Nonheme Iron Hydroxylases and Halogenases. *Catalysts*, *8*(8), 314. https://doi.org/10.3390/catal8080314

Wenkert, D., & Woodward, A. R. (1983). Studies of 2, 2'-bipyridyl N, N'-dioxides. *The Journal of Organic Chemistry*, *48*(3), 283-289.